DOI: https://doi.org/10.24425/amm.2025.154486

MIN ZHANG<sup>01</sup>, CHUN XUE<sup>01</sup>, CHUANCHUAN MA<sup>01</sup>, TUO LI<sup>01</sup>, ZHIBING CHU<sup>01\*</sup>, LEIFENG TUO<sup>01</sup>

# RESEARCH ON YIELD STRENGTH ANOMALY AND ADAPTIVE CONSTITUTIVE MODEL OF INCONEL 718 SUPERALLOY

This paper investigated the yield strength anomaly (YSA) in Inconel 718 superalloy through tensile and microstructure experiments. The study analyzed the flow behavior, examined fracture morphology, discussed dislocation distribution, and developed an adaptive constitutive model. Results show that both intermediate temperature brittleness and YSA occur at 700-800°C and strain rates of 0.01-1 s<sup>-1</sup>. This phenomenon is attributed to the influence of the intensity and content of the  $\gamma'$  phase on dislocation slip, reflecting the Kear-Wilsdorf locking mechanism. In addition, the fracture characteristics and dislocation distribution vary with temperature and strain rate. The modified Johnson-Cook model effectively predicts yield strength and plastic deformation, with advantages in wide temperature applicability (25-1000°C) and explicit YSA incorporation.

Keywords: Nickel-based superalloy; yield strength anomaly; flow behavior; fracture morphology; constitutive model

# 1. Introduction

Nickel-based superalloys can work for a long time under a high temperature of 600°C and some stress. Their structural composition and mechanical properties remain stable at temperatures below this threshold [1-3]. As a result, nickel-based superalloys are primarily used in high-temperature operating applications, such as airplane engines and nuclear reactors [4,5]. Given their stringent property requirements, research into the material properties of these superalloys is essential.

In practical production, temperature variation is unavoidable during the continuous deformation process of nickel-based superalloys. Some scholars conducted tensile experiments and identified two significant characteristics: intermediate temperature brittleness (ITB) and yield strength anomaly (YSA). For instance, Sheng et al. [6] found these phenomena at 760 and 700°C in IN792 superalloy. It indicates that the mechanical properties of nickel-based superalloys are susceptible to temperature. Additionally, superalloys are prone to brittle fracture during actual plastic deformation. Therefore, it is worthwhile to study the impact of temperature on the properties of superalloys. Scholars have engaged in extensive discussions regarding the causes of ITB and YSA in metallic materials, including the glide of dissociated super dislocations [7] and the transformation of the interaction between dislocations and  $\gamma'$  phase [8].

Some scholars have used classical constitutive models for metallic materials to predict the properties of nickel-based superalloys. For example, Huang et al. [9] refined the classical Johnson-Cook (JC) constitutive model to forecast the flow behavior of IN718 at  $400\sim600^{\circ}$ C and  $10^{-4}\sim10^{-2}$  s<sup>-1</sup>. Li et al. [10] developed a JC and Hensel Spitzel (HS) combined model to predict the flow behavior of GH3230 at 850~1000°C and 0.001~0.2 s<sup>-1</sup>. Xu et al. [11] adopted a piecewise model based on Arrhenius-type equations to describe the flow behavior of IN750H at 720~780°C. Most of the reported models for nickelbased superalloys are limited to a narrow temperature range, primarily focusing on moderate or high temperatures. Furthermore, the YSA observed during tensile experiments belongs to test uncertainty rather than inherent properties of the material [12]. Consequently, the classical constitutive models seldom give adequate consideration to the YSA.

This paper presents a comprehensive study of YSA and develops a material constitutive model tailored for this characteristic. A series of tensile experiments were conducted to investigate the effects of temperature and strain rate on mechanical properties. Morphological analysis helps to understand the formation of the ITB and YSA. Performance research laid the foundation for the construction of the material model. The resulting model can predict the mechanical properties of the Inconel 718 superalloy in a wide temperature range while adequately considering the YSA.

<sup>\*</sup> Corresponding author.chuzhibing@tyust.edu.cn



<sup>1</sup> TAIYUAN UNIVERSITY OF SCIENCE AND TECHNOLOGY, SCHOOL OF MATERIALS SCIENCE AND ENGINEERING, TAIYUAN 030024, CHINA

# 2. Experiments

The research materials utilized in this study are hot-rolled Inconel 718 superalloy sheets due to their representative microstructure and mechanical properties that closely resemble industrial processing conditions. The initial microstructure features equiaxed austenite grains with an average grain size of 22.35  $\mu$ m, as shown in Fig. 1a. The EDS map in Fig. 1b shows that its chemical component (wt.%) is 52.0Ni-17.2Cr-2.9Mo-5.1Cb (Nb) -1.00Ti-0.50Al-17.3Fe.

Given the stable performance characteristics of Inconel 718 superalloy below 600°C, tensile experiments are conducted at temperatures of 25 (room temperature, RT), 600, 700, 750, 800, 900, and 1000°C, utilizing strain rates of 0.01, 0.1, and 1 s<sup>-1</sup>. In Fig. 2a, the hot tensile experiments select standard specimens with a thickness of 3 mm and a gauge length of 35 mm, performed on a Gleeble 3800 thermal simulation testing machine. The testing parameters include a heating rate of 100°C/s, a holding time of 1 minute, and water cooling. In Fig. 2b, the RT tensile experiments select specimens with a thickness of 1 mm and a gauge length of 16 mm, performed on a WDW-10H universal testing machine. The fracture morphology is observed using ZEISS scanning electron microscopy (SEM). The distribution of dislocations is observed using JEM-F200 transmission electron microscopy (TEM). The constitutive model commonly adopts and modifies the JC model.

#### 3. Results and discussion

This paper investigates the hot tensile properties, focusing on mechanical properties (section 3.1) and fracture behavior (section 3.2). In addition, section 3.3 presents a material model constructed based on the mechanical properties to predict flow behavior.

# 3.1. Mechanical properties

The stress-strain curves typically exhibit distinct stages: the work hardening stage (WH stage), transition stage, softening stage, and fracture stage. As shown in Fig. 3a, temperature significantly influences the flow behavior. In the first temperature stage (25~700°C), the temperature has little effect on mechanical properties, reflected in the constant yield strength and sudden fracture. In the second temperature stage (750~800°C), the curves in the necking and softening stages become increasingly noticeable. In the third temperature stage (900~1000°C), the curves in the transition and softening stages gradually flatten, with noticeable local necking. Therefore, the effect of work hardening (WH) weakens with increasing temperature, while the effects of dynamic recovery (DRV) and dynamic recrystallization (DRX) increase [13]. Moreover, yield strength increases with strain rate, although the effect varies at different temperatures, as shown in

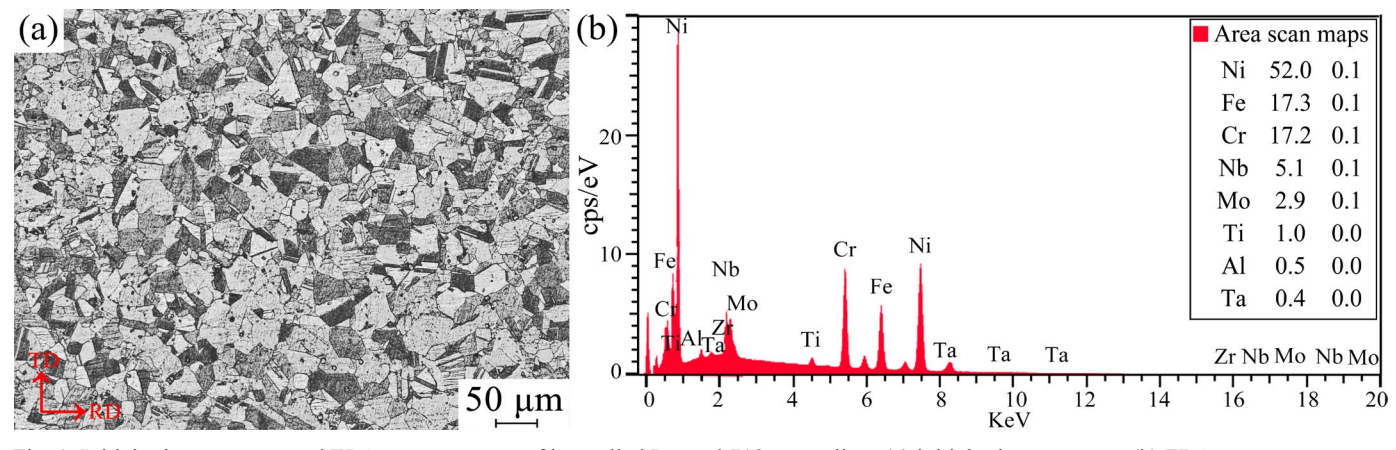


Fig. 1. Initial microstructure and EDS area scan map of hot-rolled Inconel 718 superalloy: (a) initial microstructure; (b) EDS area scan map

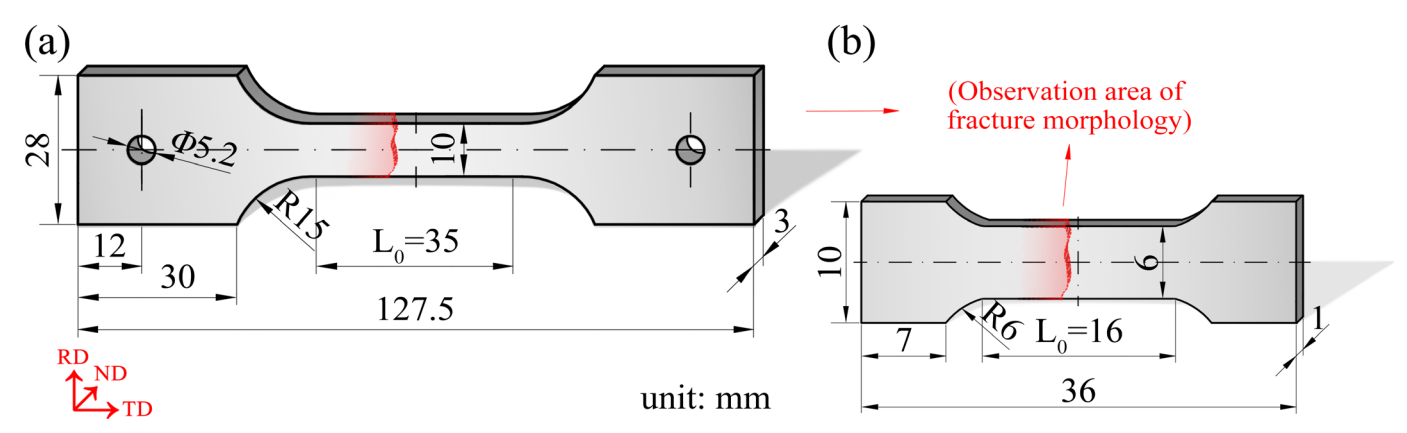


Fig. 2. the specimens for hot tensile and RT tensile experiments: (a) hot tension; (b) RT tension

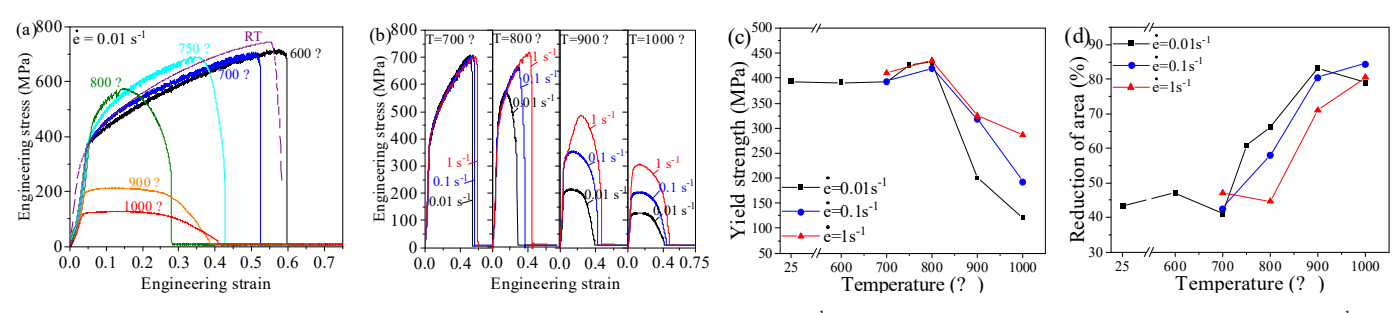


Fig. 3. A series of mechanical performance curves: (a) stress-strain curves at  $0.01 \, \mathrm{s}^{-1}$ ; (b) stress-strain curves at  $600 \sim 1000 \, ^{\circ}\mathrm{C}$  and  $0.01 \sim 1 \, \mathrm{s}^{-1}$ ; (c) yield strength-temperature at  $0.01 \sim 1 \, \mathrm{s}^{-1}$ ; (d) reduction of area-temperature at  $0.01 \sim 1 \, \mathrm{s}^{-1}$ 

Fig. 3b. Therefore, there is a coupling effect among plastic strain, strain rate, and temperature. As the temperature increases, the temperature softening effect becomes more pronounced, while the strain rate strengthening effect gradually weakens.

Generally, the strength of metallic materials decreases while their plasticity increases with rising temperature and decreasing strain rate [14]. As shown in Figs. 3c and 3d, the overall trends in yield strength and reduction of area for the nickel-based superalloy confirm this observation. However, both properties exhibit anomalous variations at 700-800°C, corresponding to the YSA and ITB [6-8]. Additionally, Fig. 3a indicates that the slope of the curve in the transition stage increases with temperature at 700~800°C.

# 3.2. Fracture behavior

In the fracture morphology of Fig. 4, the specimen width at the fracture location significantly decreases with temperature. The fracture morphology changes sequentially from pure shear fracture to serrated fracture to straight fracture. In micro, the fracture mode transitions from intergranular fracture to transgranular fracture. Due to temperature softening, the fracture surface evolves from a mixed ductile/brittle fracture surface to a predominant ductile fracture surface. Additionally, the shape and size of dimples undergo significant changes.

At 25~700°C, the fracture surface exhibits cleavage features, voids, and small shallow dimples. The dimples consist of

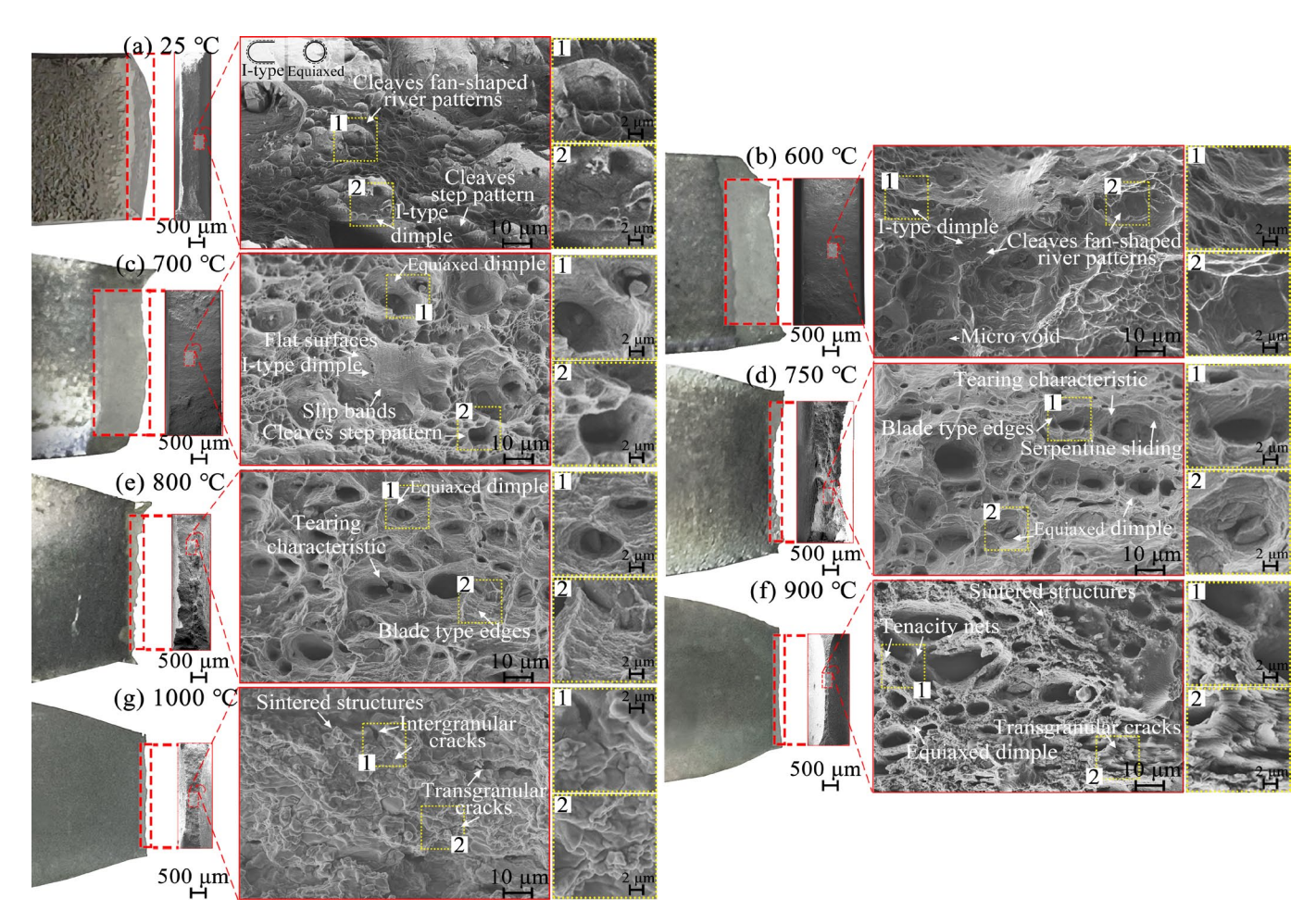


Fig. 4. Macroscopic and microscopic fracture morphology under 0.01 s<sup>-1</sup> at various temperatures: (a) 25°C; (b) 600°C; (c) 700°C; (d) 750°C; (e) 800°C; (f) 900°C; (g) 1000°C

equiaxed dimples formed by normal stress and I-type dimples formed by shear stress [15]. At 750~800°C, large and deep equiaxed dimples cover the fracture surface, while the I-type dimples and cleavages nearly disappear. At 900~1000°C, the fracture surface shows some sintering structures. Most dimples aggregate and even form tenacity nets. The transgranular fracture occurs in the local area. As the temperature increases, DRV and DRX behaviors promote further softening and improve material plasticity [16]. This improvement in plasticity is reflected in the changes in dimple morphology, including their formation, growth, and aggregation.

Difference strain rates lead to variations in fracture morphology, particularly at 800°C. At a strain rate of 0.01 s<sup>-1</sup> (Fig. 4d), the fracture surface is predominantly characterized by dimples. As the strain rate increases (Fig. 5), both the size and quantity of dimples decrease, while cleavages emerge and progressively increase. The decrease in material plasticity at higher strain rates occurs because the faster deformation rate leaves less time for plastic flow to develop [17].

# 3.3. Study on the causes of YSA

Plastic deformation in materials is closely related to dislocation motion [18,19]. The  $\gamma'$  phase, a strengthening phase in nickelbased superalloys, has a face-centered cubic structure [20] and a slip system of <110>{111} [21]. The precipitation and dissolution temperatures of the  $\gamma'$  phase are approximately 593 and 843°C, respectively [22]. At 600°C (Fig. 6a), the  $\gamma'$  phase is relatively small. Some dislocations cut through  $\gamma'$  phase. At 800°C (Fig. 6b), the  $\gamma'$  phase reaches its maximum precipitation, characterized by large size, high content, and narrow spacing. Due to the intensity of the  $\gamma'$  phase increases with temperature [23], dislocations cannot cut through it. Instead, dislocations undergo multiple climbs and cross-slips within the matrix  $\gamma$  phase, resulting in local slip

from the  $\{111\}$  to  $\{100\}$  planes. Therefore, the YSA is mainly attributed to the Kear-Wilsdorf (K-W) locking mechanism, which occurs when dislocations cross-slip on non-slip crystallographic planes [24], hindering dislocation motion. At 900°C (Fig. 6c), the  $\gamma'$  phase dissolves almost completely. Thermal activation facilitates dislocation motion, which reduces dislocation density and enhances the toughness of the matrix phase.

#### 3.4. Constitutive models of hot tensile behavior

Developing a constitutive model that accurately represents the properties of Inconel 718 superalloy is challenging. For instance: (1) the YSA prevents the yield strength from decreasing monotonically with temperature; (2) significant variations in the softening stage are directly reflected in the slope changes of the stress-strain curves.

Before constructing the model, convert the engineering stress-strain data into the true one.

$$\sigma = \sigma_e (1 + \varepsilon_e)$$
$$\varepsilon = \ln(1 + \varepsilon_e)$$

where  $\sigma$  and  $\sigma_e$  are the true stress and engineering stress, respectively;  $\varepsilon$  and  $\varepsilon_e$  are the true strain and engineering strain, respectively.

Given the classic JC model [13] in Eq. (1), its basic formula is  $A + B\varepsilon^n$ .

$$\sigma = (A + B\varepsilon^n)(1 + C\ln\dot{\varepsilon}^*)(1 - T^{*m}) \tag{1}$$

where:

$$\dot{\varepsilon}^* = \frac{\dot{\varepsilon}}{\dot{\varepsilon}_0}, \dot{\varepsilon}$$
 is the reference strain rate;

$$T^{*m} = \frac{T - T_r}{T_m - T_r}$$
,  $T_r$  is the reference temperature,  $T_m$  is the dissolution temperature equal to 1320°C.

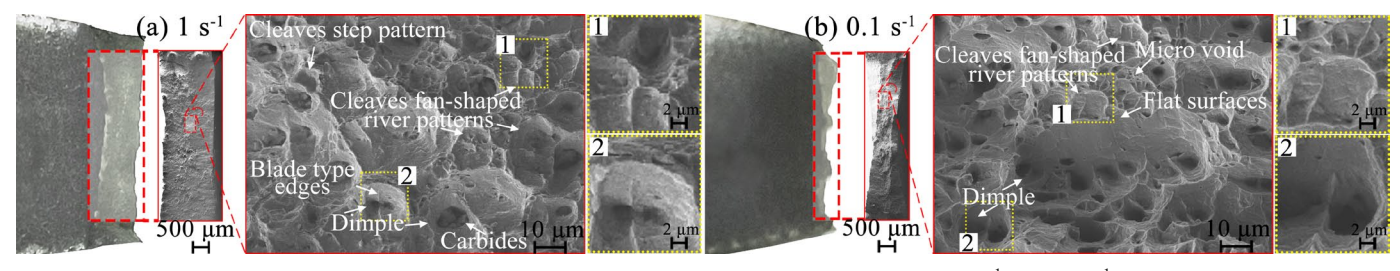


Fig. 5. Macroscopic and microscopic fracture morphology at 800°C under various strain rates: (a) 1 s<sup>-1</sup>; (b) 0.1 s<sup>-1</sup>

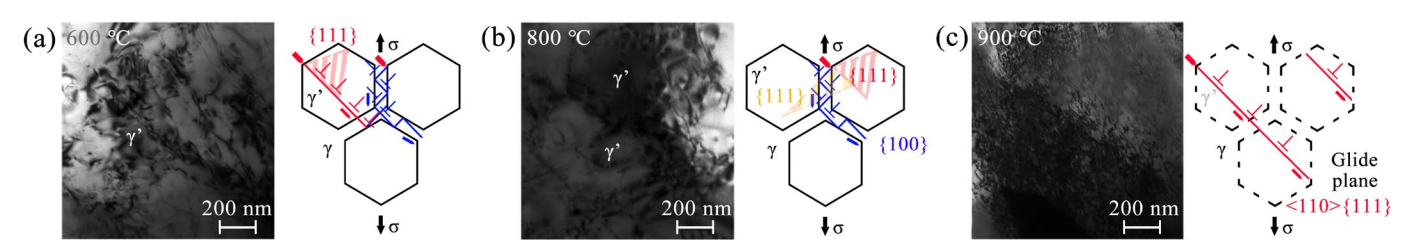


Fig. 6. TEM observation and schematic diagram of dislocation distribution at different temperatures: (a) dislocations cut through the  $\gamma'$  phase at 600°C; (b) multiple climbing and cross-sliping at 800°C; (c) dislocations flow easily at 900°C

Expand Eq. (1) to obtain Eq. (2).

$$\sigma = A(1 + C \ln \dot{\varepsilon}^*)(1 - T^{*m}) + B(1 + C \ln \dot{\varepsilon}^*)(1 - T^{*m})\varepsilon^n \quad (2)$$

In Eq. (2), the yield strength typically decreases with temperature, which contradicts the YSA observed in the experiments. Therefore, the yield strength and plastic deformation in the constitutive model respond differently to temperature and strain rate changes. To capture this divergence, Eq. (3) employs parameters  $\sigma_0(T, \dot{\varepsilon})$  and  $G(T, \dot{\varepsilon})\varepsilon^n$  to replace  $A(1 + C \ln \dot{\varepsilon}^*)(1 - T^{*m})$  and  $B(1 + C \ln \dot{\varepsilon}^*)(1 - T^{*m})\varepsilon^n$  for precise modeling.

$$\sigma = \sigma_0(T, \dot{\varepsilon}) + G(T, \dot{\varepsilon})\varepsilon^n \tag{3}$$

where  $\sigma_0$  is the yield strength, its calculation needs to take into account the impact of YSA;  $F(\varepsilon)$  is the basic formula for characterizing the plastic deformation stage; G is the influencing parameter in the plastic deformation stage.

#### 3.3.1. Yield stress calculation

Inconel 718 superalloy is a precipitation-hardening superalloy, and its strength is primarily influenced by the precipitation phase. Combining the K-W locking mechanism, the calculation of yield strength focuses on the phase precipitation and dislocation motion. Cross-slip, which is highly temperature-dependent, exhibits Gaussian distribution characteristics [25]. Eq. (4) [25] represents the possibility of cross-slip as follows:

$$p = \exp[D|T - T_0|] \tag{4}$$

where  $T_0$  is the original temperature, with the most prominent K-W lock and YSA, equal to 800°C; D is material parameters.

Cross-slip causes shear stress. The relationship between shear stress and yield stress is as follows:

$$\sigma_0 = p \frac{\tau}{S} \tag{5}$$

where  $\tau$  is shear stress of cross slip; S is the Schmid factor.

Replace 
$$\frac{\tau}{S}$$
 with  $[A + B \exp(CT)]$ . Combining Eq. (4) and

considering the effects of temperature and strain rate on the yield strength, rewrite Eq. (5) as follows:

$$\sigma_0(T, \dot{\varepsilon}) = [A + B \exp(CT)]$$

$$\exp[D(\dot{\varepsilon}) | T - T_0 |] (1 + E(\dot{\varepsilon}) \cdot T^* \cdot \ln \dot{\varepsilon}^*)$$
(6)

where A, B, C, D and E are material parameters. Due to the coupling effect of temperature and strain rate, D and E are affected by strain rate.

By fitting the experimental data, the following yield strength expression is obtained.

$$\sigma_{0}(T, \dot{\varepsilon}) = [0.14 + 17.7 \exp(-0.0038T)]$$

$$\exp\left[ (-47.2(\ln \dot{\varepsilon})^{2} - 389.3 \ln \dot{\varepsilon} - 1062) | T - 800 | \right]$$

$$\left( 1 + (-0.07036 \ln \dot{\varepsilon} + 0.268) \cdot \frac{T - 800}{1320 - 8000} \cdot \ln \frac{\dot{\varepsilon}}{0.01} \right) \quad (7)$$

Fit the yield strength-temperature  $(\sigma_0 - T)$  curves in Fig. 7.

# 3.3.2. Stress calculation during the plastic deformation stage

This section simulates the stress-strain curve during the plastic deformation stage. In Fig. 3, the slope of stress-strain curve during the plastic deformation stage is approximately equal to 1 at low and intermediate temperatures, and is approximately equal to 0 at high temperatures. The G value shows a sudden change with temperature. Therefore, the S-shaped growth function (Eq. (8)) is more suitable for expressing the slope than  $(1 + C \ln \dot{\epsilon}^*)(1 - T^{*m})$ . Fit Eq. (3) as follows:

$$G(T, \dot{\varepsilon}) = \frac{a}{1 + \exp[k(T - T_c)]}$$
 (8)

$$G(T, \dot{\varepsilon}) = \frac{1900}{1 + \exp[-0.02(T - 900 - 70 \cdot \ln \dot{\varepsilon} / \ln 10)]}$$
(9)

$$n = 2.7 + 0.1 \cdot \ln \dot{\varepsilon} / \ln 10 - 0.0024 \cdot T \quad (n \le 1)$$
 (10)

The fitting curve in Fig. 8 demonstrates that the model can accurately predict the actual stress-strain curve of Inconel 718 superalloy. This model not only quantitatively captures the YSA, but also illustrates the effects of temperature and strain rate on plastic deformation characteristics.

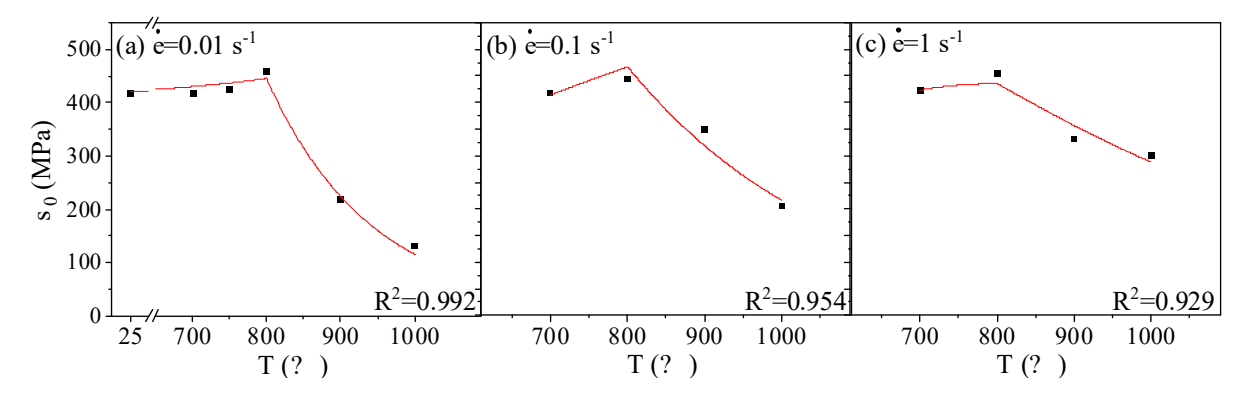


Fig. 7. Fitting diagram of stress-temperature  $(\sigma_0 - T)$  curves at various strain rates: (a)  $\dot{\varepsilon} = 0.01 \text{ s}^{-1}$ ; (b)  $\dot{\varepsilon} = 0.1 \text{ s}^{-1}$ ; (c)  $\dot{\varepsilon} = 1 \text{ s}^{-1}$ 

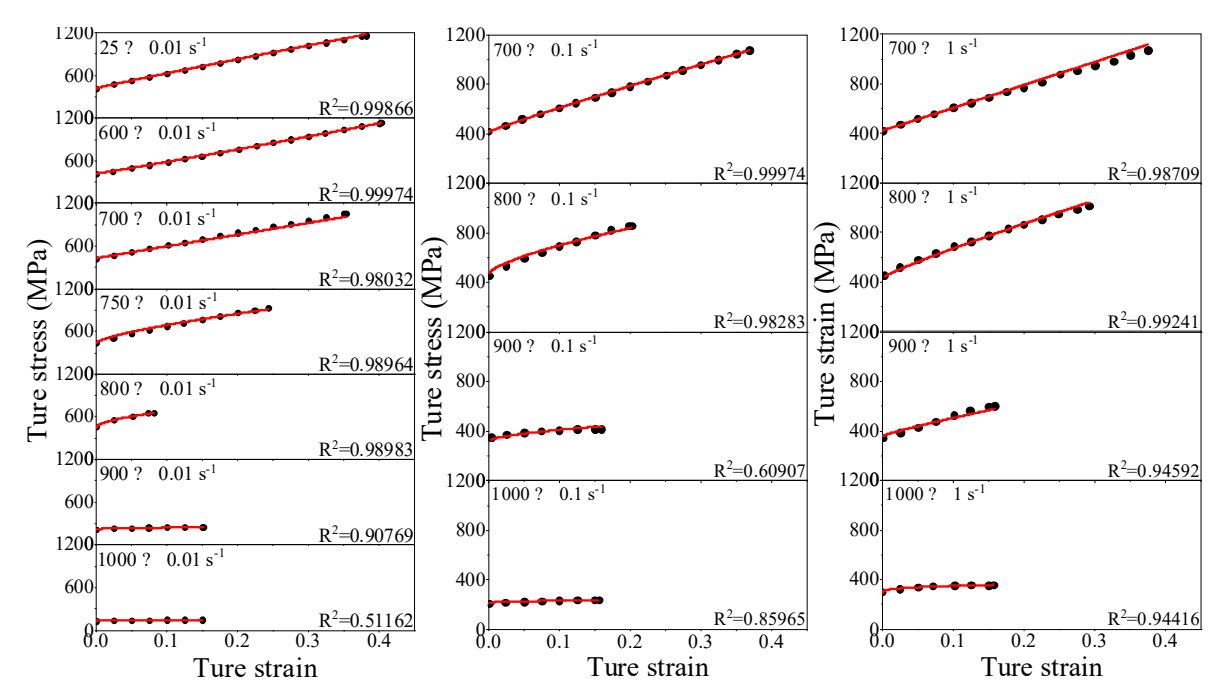


Fig. 8. Stress-strain curve fitting map

#### 4. Conclusion

- 1. The yield strength generally decreases as the temperature rises or the strain rate decreases. In contrast, the reduction of area shows an overall increasing trend. As the temperature increases, the temperature softening effect becomes more pronounced, while the strain rate strengthening effect gradually weakens. In addition, the ITB and YSA occur at a temperature of 700~800°Cand a strain rate of 0.01~1 s<sup>-1</sup>.
- 2. As the temperature increases, the fracture surface changes from a mixed ductile/brittle fracture to a ductile fracture and shifts from intergranular fracture to transgranular fracture. In addition, changes in the intensity and content of the  $\gamma'$  phase affect dislocation slip, promoting the K-W locking mechanism at intermediate temperatures, which leads to ITB and YSA. In contrast, an increase in strain rate suppresses dimple formation and growth.
- 3. The modified model consists of yield strength part and plastic deformation part. The former introduces the K-W locking mechanism to expand the temperature range without ignoring YSA. The latter uses an S-shaped growth function to capture the abrupt change in the temperature's effect on the transition stage. Compared to experimental data, the model can accurately predict material flow behavior.

# Acknowledgments

This work was supported by the National Natural Science Foundation of China [grant number 52175353]; the Shanxi Province Key Research and Development Program [grant number 202102150401002]; and the Shanxi Province Major Science and Technology Special Project [grant number 202101110401009].

### REFERENCES

- Intermediate Temperature Brittleness Mechanism of Inconel 625
   Deposited Metal. J. Mater. Res. Technol. 17, 1812-1821 (2022).
   DOI: https://doi.org/10.1016/j.jmrt.2022.01.143
- [2] D.W. Han, L.X. Yu, F. Liu, B. Zhang, W.R. Sun, Effect of Heat Treatment on the Microstructure and Mechanical Properties of the Modified 718 Alloy. Acta Metal. Sin. Engl. 31, 1224-1232 (2018).
  - DOI: https://doi.org/10.1007/s40195-018-0790-9
- [3] J.T. Chen, J.X. Lu, W. Cai, Y.F. Zhang, Y.F. Wang, W.X. Jiang, M. Rizwan, Z. Zhang, In-situ Study of Adjacent Grains Slip Transfer of Inconel 718 during Tensile Process at High Temperature. Int. J. Plasticity 163, 103554 (2023).
  POLyhttps://doi.org/10.1016/j.iinleg.2022.102554
  - DOI: https://doi.org/10.1016/j.ijplas.2023.103554
- [4] G.F. Xiao, Q.X. Xia, Y.L. Zhang, X.Q. Cheng, Manufacturing of Ni-based superalloy thin-walled components by complex strainpath spinning combined with solution heat treatment. Int. J. Adv. Manuf. Tech. 117, 199-215 (2021).
  - DOI: https://doi.org/10.1007/s00170-021-07676-1
- [5] C. Zhang, L.M. Yu, H. Wang, Kinetic Analysis for High-temperature Coarsening of γ" Phase in Ni-based Superalloy GH4169. Materials 12, 2096 (2019).
  DOLL https://doi.org/10.2300/ps.121222006
  - DOI: https://doi.org/10.3390/ma12132096
- [6] B.N. Du, L.Y. Sheng, Z.Y. Hu, C.Y. Cui, J.X. Yang, X.F. Sun, Investigation on the Microstructure and Tensile Behavior of a Nibased IN792 Superalloy. Adv. Mech. Eng. 10, 1-8 (2018). DOI: https://doi.org/10.1177/1687814017752167
- [7] N. Yurchenko, E. Panina, A. Belyakov, G. Salishchev, S. Zherebtsov, N. Stepanov, On the Yield Stress Anomaly in a B2-ordered Refractory AlNbTiVZr0.25 High-entropy Alloy. Materials Letters 311, 131584 (2022).
  - DOI: https://doi.org/10.1016/j.matlet.2021.131584

- [8] H. Shang, Q.S. Ma, Q.Z. Gao, H.L. Zhang, H.J. Li, H.J. Zhang, L.L. Sun, Yield Strength Anomaly Evaluation of W-free Co-Ni-Al-based Superalloys during High Temperature Tensile Tests. Mater. Charact. 192, 112242 (2022). DOI: https://doi.org/10.1016/j.matchar.2022.112242
- [9] N.Y. Xi, X.W. Fang, Y.S. Duan, Q. Zhang, K. Huang, Wire Arc Additive Manufacturing of Inconel 718: Constitutive Modelling and Its Microstructure Basis. Journal of Manufacturing Processes 75, 1134-1143 (2022).
  - DOI: https://doi.org/10.1016/j.jmapro.2022.01.067 23J14
- [10] Y.Q. Chen, H. Li, S. Zhang, J. Luo, J.F. Teng, Y.L. Lv, M.Q. Li, Hot Tensile Deformation Behavior and Constitutive Models of GH3230 Superalloy Double-sheet. Materials 16, 803 (2023). DOI: https://doi.org/10.3390/ma16020803
- [11] K.M. Wang, H.Y. Jing, L.Y. Xu, Y.D. Han, L. Zhao, B. Xiao, S.Q. Yang, A Piecewise Constitutive Model, Microstructure and Fracture Mechanism of a Nickel-based Superalloy 750H during High-temperature Tensile Deformation. Journal of Materials Science 54, 9775-9796 (2019). DOI: https://doi.org/10.1007/s10853-019-03566-w
- [12] L. Zheng, G. Schmitz, Y. Meng, R. Chellali, R. Schlesiger, Mechanism of Intermediate Temperature Embrittlement of Ni and Ni-based Superalloys. Crit. Rev. Solid State 37, 181–214 (2012). DOI: https://doi.org/10.1080/10408436.2011.613492
- [13] Y.C. Lin, X.M. Chen, A Critical Review of Experimental Results and Constitutive Descriptions for Metals and Alloys in Hot Working. Materials and Design 32, 1733–1759 (2011). DOI: https://doi.org/10.1016/j.matdes.2010.11.048
- [14] J.H. Wang, L. Zhang, P.P. Jin, L.J. Chen, X.G. Yuan, H.B. Ma, Microstructure Evolution and Constitutive Relation Establishment of Extruded Mg-1Al-6Y Alloy under High Speed Impact. Journal of Alloys and Compounds 908, 164540 (2022). DOI: https://doi.org/10.1016/j.jallcom.2022.164540
- [15] Q.P. Zhong, Z.H. Zhao, Fractography. Beijing: Higher Education Press, 2006 (In Chinese).
- [16] D.X. Wen, T.Y. Yue, Y.B. Xiong, K.Wang, J.K. Wang, Z.Z. Zheng, J.J. Li, High-temperature Tensile Characteristics and Constitutive Models of Ultrahigh Strength Steel. Materials Science and Engineering A 803, 140491 (2021). DOI: https://doi.org/10.1007/s12540-020-00944-x
- [17] H. Mei, L.H. Lang, X.G. Yang, Z. Liu, X.X. Li, Study on Constitutive Relation of Nickel-Base Superalloy Inconel 718 Based

- on Long Short Term Memory Recurrent Neural Network. Metals **10**, 1588 (2020).
- DOI: https://doi.org/10.3390/met10121588
- [18] H.J. Pan, X.Y. Li, H.M. Zhang, L. Liu, J. Li, Y.J. Zhao, Z.J. Wang, Y. Zhang, Z.Q. Wu, M.H. Cai, H. Ding, Achieving Ultra-high Elongation of 1401% in a Warm-rolled Medium Mn Lightweight Steel with Dual-phase Lamellar Structure. Mat. Sci. Eng. A 862, 144493 (2023).
  - DOI: https://doi.org/10.1016/j.msea.2022.144493
- [19] A.Q. Liu, F. Zhao, W.S. Huang, Y.B. Tan, Y.H. Ren, L.X. Wang, F.H. Xu, Effect of Aging Temperature on Precipitates Evolution and Mechanical Properties of GH4169 Superalloy. Crystals 13, 964 (2023).
  - DOI: https://doi.org/10.3390/cryst13060964
- [20] M. Mohr, R. Wunderlich, Y. Dong, D. Furrer, H.J. Fecht, Thermophysical Properties of advanced Ni-Based Superalloys in the Liquid State Measured on Board the International Space Station. Advanced Engneering Materials 22, 1901228 (2020). DOI: https://doi.org/10.1002/adem.202070016.
- [21] Y.M. Li, Z.H. Tan, X.G. Wang, Y. Mu, H.C. Zhao, H.B. Tan, J.L. Liu, B. Wang, J.G. Li, Y.Z. Zhou, X.F. Sun, Stress Rupture Anisotropy of a Ru-containing Fourth-generation Single Crystal Superalloy at 760°C and 1100°C. Mat Sci Eng A 856, 144006 (2022). DOI: https://doi.org/10.1016/j.msea.2022.144006
- [22] L.Y. Sheng, F. Yang, J.T. Guo, T.F. Xi, Anomalous Yield and Intermediate Temperature Brittleness Behaviors of Directionally Solidified Nickel-based Superalloy. T. Nonferr. Metal. Soc. 24, 673-681 (2014).
  - DOI: https://doi.org/10.1016/s1003-6326(14)63110-1
- [23] J.J. Wang, W.G. Guo, Y. Su, P. Zhou, K.B. Yuan, Anomalous Behaviors of a Single-crystal Nickel-base Superalloy over a Wide Range of Temperatures and Strain Rates. Mechanics of Materials 94, 79-90 (2016).
  - DOI: https://doi.org/10.1016/j.mechmat.2015.11.015
- [24] K.V. Vamsi, S. Karthikeyan, Deformation Modes and Yield Strength Anomaly in L12 Compounds. Journal of Alloys and Compounds 860, 158411 (2021). DOI: https://doi.org/10.1016/j.jallcom.2020.158411
- [25] Y. Wang, Y.X. Zhou, Y.M. Xia, A Constitutive Description of Tensile Behavior for Brass over a Wide Range of Strain Rates. Mat. Sci. Eng. A 372, 186-190 (2004). DOI: https://doi.org/10.1016/j.msea.2003.12.009